Roles of carbon chain and functional group of perfluoroalkyl acids and novel alternatives in adsorption on metal-organic frameworks: insights into mechanism and adsorption prediction

Hao Guo [a], Tongyu Hu [b], Feng Xiao [c], Zhaoyang Liu [a,*], Andrew J. Sweetman [d], Chenchen Qu [a], Fayang Guo [e], Jingtao Hou [a], Jay Gan [f], Wenfeng Tan [a]

[a] *State Environmental Protection Key Laboratory of Soil Health and Green Remediation, College of Resources and Environment, Huazhong Agricultural University, Wuhan 430070, China*

[b] *BCEG Environmental Remediation Co., Ltd., Beijing 100101, China*

[c] *Department of Civil and Environmental Engineering, University of Missouri, Columbia, MO 65211, USA*

[d] *Lancaster Environment Centre, Lancaster University, Lancaster LA1 4YQ, UK*

[e] *Institute of Resource and Environment, Henan Polytechnic University, Jiaozuo 454000, China*

[f] *Department of Environmental Sciences, University of California, Riverside, CA 92521, USA*

*Corresponding author: Zhaoyang Liu, Tel: 86-27-87287508, Fax: +86-27-87288618, E-mail: zhaoyangliu@mail.hzau.edu.cn

Abstract: Legacy hazardous perfluoroalkyl acids (PFAAs) are being replaced by short-chain homologs and novel alternatives. To determine the effects of varying carbon chains and functional groups of these emerging contaminants on adsorption behavior, this study has systematically revealed the structure-adsorption relationships and interaction mechanisms of different PFAAs and alternatives (collectively named as per- and polyfluoroalkyl substances, PFAS) on a metal-organic framework (MOF) MIL-101(Cr), and thus proposed a parameter representing the average unit electronegativity of PFAS for adsorption prediction. Long-chain, branched, or carboxylate-based PFAS showed higher adsorption capacities on MIL-101(Cr) than the corresponding short-chain, linear, or sulfonate-based counterparts, respectively. The ether bond introduction to PFAS increased the adsorption capacity, whereas replacing C-F units of PFAS with C-H units caused a decrease in adsorption. The adsorption of different structural PFAS on MIL-101(Cr) was mainly governed by electrostatic interaction, complexation, hydrogen bonding, π-CF, and π-anion as well as steric effects, which were associated with the molecular electronegativity and PFAS chain length. The average unit electronegativity of individual PFAS was estimated and found to show significantly positive correlations with their adsorption capacities and removal rates by MIL-101(Cr), which may assist with the adsorption prediction of various PFAS on MOF materials.

Key words: PFAS; MIL-101(Cr); structure-adsorption relationship; interaction mechanism; unit electronegativity; adsorption prediction.

41 **1. Introduction**

42 The ubiquitous occurrence of perfluoroalkyl acids (PFAAs) in the environment
43 after several decades of manufacturing and various consumer uses has resulted in global
44 concern (Li et al. 2022). Particular attention has been directed at legacy long-chain
45 PFAAs, such as perfluorooctane sulfonic acid (PFOS) and perfluorooctanoic acid
46 (PFOA), due to their severe hazardous effects on human health (Joerss et al. 2020). As
47 tightening regulation of these long-chain PFASs, different alternative strategies have
48 been developed to meet expanding market demands, such as shortening carbon chains
49 (e.g., perfluorohexanoic acid, PFHxA), ether bond introduction (e.g.,
50 hexafluoropropylene oxide dimeric acid, HFPO-DA, trade name GenX) and hydrogen
51 substitution of fluorine (e.g., 6:2 fluorotelomer sulfonate, 6:2 FTS). However, adverse
52 effects of these alternatives to human and ecological health have also been emerging
53 (Gomis et al. 2018, Ma et al. 2022). Water bodies have been identified as a major
54 environmental sink and critical human exposure pathway of PFAAs and alternatives
55 (Wang et al. 2023).

56 Numerous efforts have been devoted to the removal of PFAAs from water such
57 as adsorption, reverse osmosis, enhanced photolysis, electrochemical oxidation, and
58 microwave degradation (Deng et al. 2015, Wang et al. 2019). Considering the refractory
59 degradation of PFAAs due to strong intramolecular C-F bonds (485 kJ/mol) (Cheng et
60 al. 2014), adsorption has become a promising strategy for efficiently removing these
61 chemicals. The adsorption of PFOS and PFOA by conventional materials, such as

activated carbon, ion exchange resin, clay, and chitosan, has been extensively studied (Peng et al. 2017). While the research on the removal of shorter-chained homologs and novel alternatives, such as GenX and 6:2 FTS, also requires attention (Fang et al. 2023).

Metal-organic frameworks (MOFs) are a new class of hybrid crystalline porous materials with unsaturated metal sites, large specific surface area (SSA) and superior pore structure, rendering MOFs promising adsorption candidates of PFAAs and alternatives (Yu et al. 2023). The removal capacities for single MOFs for PFOA (e.g., Zn-based microporous framework, ZIF) and PFOS (e.g., Th-based mesoporous framework, SCU) have been investigated (Li et al. 2017, Rosler et al. 2016), but the roles of the carbon chain and functional group (such as carboxylate, sulfonate, ether bond, and hydrocarbon bond) of different PFAAs and novel alternatives in adsorption performance and mechanism on MOFs remain largely unknown (Li et al. 2023). PFAA production is mainly based on an electrochemical fluorination process, and generally yields a mixture of linear and branched isomers, which could exhibit isomer-specific adsorption behaviors (Nickerson et al. 2021, Schulz et al. 2020). Studying the differential adsorption performance between linear and branch PFAA isomers will contribute to an improved understanding of the adsorption behavior of these chemicals. In addition, mechanism based adsorption performance prediction according to different structural PFAAs and alternatives on MOFs is still uncommon, but would facilitate the design of high-performance MOFs based on profiles of environmental PFAAs and alternatives.

83 As a representative MOF, MIL-101(Cr) is charactered by a stable structure with
84 abundant interaction sites and large SSA, and has shown high adsorption potentials for
85 PFOA and PFOS (Lu et al. 2016, Zhao et al. 2021). To fill above-mentioned knowledge
86 gaps, this study used MIL-101(Cr) as an example MOF, and aimed to assess the roles
87 of the carbon chain and functional group of PFAAs and novel alternatives (collectively
88 as per- and polyfluoroalkyl substances, PFAS) in their adsorption on MOFs, followed
89 by the exploration of adsorption performance prediction based on the molecular
90 properties of different PFAS. Specific objectives included (i) determination of the
91 differential adsorption kinetics and capacities of PFAS with varying carbon chains and
92 functional groups (e.g., carboxylate, sulfonate, ether bond and hydrocarbon bond); (ii)
93 identification of the adsorption performance of different PFAS responding to the
94 changes of solution pH, and ionic species (cation and anion) and strengths; (iii)
95 identification of the adsorption mechanism, followed by normalization of an effective
96 indicator of differential PFAS to predict their adsorption performance; and (iv)
97 investigation of the removal of various PFAS and isomers in natural water and
98 regeneration potentials. To the best of our knowledge, this study represents one of the
99 first attempts to assess the effect of changes in carbon chain and functional group of
100 PFAS on their adsorption on MOF, with the goal to achieve adsorption performance
101 prediction for a range of different PFAS.

102 **2. Materials and methods**

103 **2.1 Preparation and characterization of MIL-101(Cr)**

3.39 g of H_2BDC (>98%) and 8.16 g of $Cr(NO_3)_3 \cdot 9H_2O$ (>98%) were added into 100 mL of Milli-Q water and stirred for 60 min. The resulting suspension was sonicated for 30 minutes at room temperature before being heated to 220 °C with a heating rate of 5 °C/min and kept for 20 h in a 200 mL Teflon-lined autoclave. After cooling to room temperature, the crude product was collected by centrifugation at 4000 rpm for 5 minutes, and sequentially washed for three times with dimethylformamide and ethanol respectively at 100 ℃ in an autoclave for 12 h. The resulting material was dried in a vacuum oven at 70 °C for 12 h to obtain the MIL-101(Cr) sample.

The prepared sample was then characterized using a scanning electron microscope (SEM) for morphology, powder X-ray diffraction (XRD) for mineral crystals, Brunauere-Emmette-Teller (BET) adsorption isotherms for SSA and pore structures, Fourier transform infrared spectroscopy (FTIR) for surface functional groups, X-ray photoelectron spectroscopy (XPS) for binding energies of different elements, and dynamic light scattering (DLS) for zeta potentials (seeing details in Supplementary Information, SI 1.1).

2.2 PFAS adsorption experiments

According to different substitution strategies for PFOA and PFOS, PFOA and its shorter-chain homolog PFHxA and ether bond-introduced alternative GenX, as well as PFOS and its hydrogen-substituted alternative 6:2 FTS were selected for the adsorption experiments. Standards of PFOA, PFHxA, PFOS, 6:2 FTS, and GenX were purchased from Macklin Biochemical Technology (Shanghai, China) (Table S1).

125 Adsorption isotherms of different PFAS were developed using standard batch
126 adsorption experiments using round-bottom polypropylene tubes with 16 μg MIL-
127 101(Cr) and 20 mL solution containing 0~7 mM of each PFAS and 2 mM of NaH_2PO_4
128 as buffer ions, followed by adjusting pH to 5.0 ± 0.2 with 0.1~1 M HCl/NaOH. The
129 tubes were sealed and shaken at 200 rpm for 24 h to reach adsorption equilibrium, and
130 then centrifuged at 12000 rpm for 2 min with 1 mL supernatant being transferred into
131 sampler vials for further analysis by high-performance liquid chromatography-mass
132 spectrometer (HPLC-MS/MS). The adsorption kinetics of different PFAS (2 mM) on
133 MIL-101(Cr) were performed at 200 rpm for 1~360 min. The effects of pH changes
134 (3.0~11.0) and ionic strengths (Ca^{2+} and SO_4^{2-}) of 1~100 mM on the adsorption
135 performance of different PFAS (2 mM) were also assessed. Duplicate vials for the
136 above experiments were set up, and detailed procedures were described in SI 1.2

137 **2.3 Practical applications and recycling experiments**

138 To further examine the practical application of MIL-101(Cr) in natural waters,
139 a heavily-contaminated groundwater sample containing multiple PFAS and isomers
140 was collected nearby a fluorochemical facility in central China (seeing details in SI 1.2).
141 MIL-101(Cr) was directly added to the natural water sample with a sorbent
142 concentration of 0.8 mg/L, followed by the same procedures as those described in the
143 adsorption experiments. PFAS in water samples were extracted by solid phase
144 extraction and quantified using HPLC-MS/MS (Thermo Fisher Scientific Co., USA)
145 (Tables S2 and S3). Water quality parameters, including pH and conductance, were

146 determined in situ using an EXO3 multi-parameter sonde (Yellow Springs, Ohio, USA).
147 After the adsorption of PFAS, MIL-101(Cr) regenerations with three cycles in natural
148 water were performed by methanol solution (containing 1.25% $NaNO_3$, 1.25% NaCl,
149 1.25% Na_2SO_4 and 1.25%Na_2CO_3) and freeze-drying. The adsorption, extraction, and
150 detection of PFAS and material recycling procedures were detailly described in SI 1.2
151 and 1.3.

152 **2.4 Data analysis**

153 The adsorption data were analyzed using the Langmuir model: $Q_e =$
154 $(Q_m K_L C_e)/(1 + K_L C_e)$, where Q_e (mg/g) and C_e (mg/L) represent equilibrium sorbent
155 and solution concentrations of PFAS, respectively (the same below), Q_m (mg/g) is the
156 maximum adsorption capacity of sorbent, and K_L (L/mg) is the adsorption constant
157 associated with the affinity between sorbent and PFAS. The adsorption data were also
158 analyzed using the Freundlich model: $Q_e = K_f {C_e}^n$, where K_f ((mg/g)/(mg/L)^n) means
159 the Freundlich adsorption coefficient and n is often used as an indicator of isotherm
160 nonlinearity. The kinetic adsorption data were analyzed using the pseudo second-order
161 model, pseudo-first-order model, and intra-particle diffusion model, respectively, as
162 follows: $dq_t/q_t = k_1(q_e - q_t)$, $dq_t/q_t = k_2(q_e - q_t)^2$, and $q_t = k_i t^{0.5} + C$, where
163 q_t (μmol/g) and q_e (μmol/g) are the amounts of PFAS on sorbent at time t and when
164 reaching adsorption equilibrium respectively, k_1 (min^{-1}) and k_2 (g·μmol^{-1}·min^{-1}) are the
165 constants of the pseudo second-order model and pseudo-first-order model, respectively;
166 in intra-particle diffusion model, k_i is the diffusion rate constant (μmol/(g·h$^{0.5}$)) and C

(μmol/g) is the constant related to the thickness of boundary layer. The Gibbs free energy(ΔG) during adsorption was calculated using the following equation: $\Delta G = -RTlnK_D$, where K_D is the thermodynamic equilibrium constant and can refer to K_f in the Freundlich adsorption model.

3. Results and discussion

3.1 Micromorphology and surface chemistry of MIL-101(Cr)

The SEM images of prepared MIL-101(Cr) demonstrated a well-distributed regular octahedron, and its pattern of crystalline showed by XRD was consistent with that reported by Férey et al. (2005), who synthesized this material for the first time, suggesting the successful preparation (Fig. S1 and Fig. S2a). According to the FTIR profile of MIL-101(Cr) (Fig. S2b), the adsorption bands around 1402 and 1545 cm^{-1} were associated with -COOH of the dicarboxylate in the framework (Maksimchuk et al. 2008, Sun et al. 2014), and the vibrational band around 3440 cm^{-1} indicated the existence of -OH due to the stretching of bonded water molecules (Jia et al. 2013). These O-containing functional groups on MIL-101(Cr) may have contributed to the complexation and hydrogen bonding with the anion functional group of PFAS (Liu et al. 2022). Meanwhile, the peak bands at 1505 cm^{-1} can be assigned to aromatic rings (Liu et al. 2013), which may have exhibited a potential π-CF interaction with the CF units of PFAS. The pH_{PZC} point of MIL-101(Cr) was calculated at 6.85 based on the zeta potentials (pH: 3.0~11.0), and the material was positively charged under the solution pH (5.0 ± 0.2) of the adsorption experiments, possibly aiding the electrostatic

attraction with anionic PFAS (FitzGerald et al. 2022). The BET analysis demonstrated the SSA of MIL-101(Cr) to be as high as 2478 m^2/g and a N_2 adsorption-desorption isotherm of the typical IV-type. As shown in Fig. S2d, the adsorption and desorption branches coincided, with no obvious hysteresis loop appearing, indicating few large pore structures (Hamon et al. 2009); while the adsorption capacity increased rapidly with increasing relative pressure in the initial stage, reflecting the presence of large amounts of micropores (Fakhraie et al. 2023). The pore size distribution also demonstrated the dominance of micropores in MIL-101(Cr), which could influence the diffusion of PFAS during adsorption (Zhao et al. 2020).

3.2 Adsorption kinetics of different PFAS

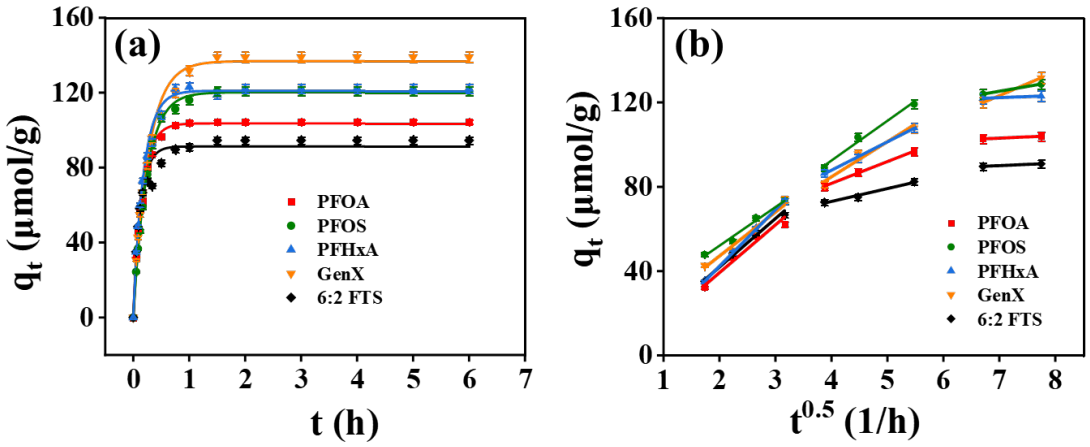

Fig. 1 Adsorption kinetics of PFOA, PFOS, PFHxA, GenX, and 6:2 FTS on MIL-101(Cr) fitted by pseudo-second-order model (a) and internal diffusion model (b) (solution pH: 5.0; initial PFAS concentration: 2 mM).

The adsorption kinetics of various PFAS on MIL-101(Cr) revealed two stages, including quick adsorption to reach approximately 80% of the equilibrium adsorption amount in the first 60 min and then slow adsorption to achieve the equilibrium after 90

min, suggesting the rapid adsorption of PFAS. As shown in Fig. 1a, the goodness of fitness (R^2>0.96) of pseudo-second-order kinetic model indicated an important role of chemical interactions in PFAS adsorption (Table S4 and Fig. S3), which could include electrostatic attraction, complexation, π-CF interactions, and hydrogen bonding (Du et al. 2014, Liu et al. 2015, Yang et al. 2020). Furthermore, based on an intraparticle diffusion model, the whole adsorption process of various PFAS may consist of membrane diffusion, intraparticle diffusion and adsorptive attachment (Piai et al. 2019), with the corresponding adsorption rate constants decreasing sequentially, indicating a gradually slower adsorption rate in above three steps (Fig. 1b and Table S5). Moreover, the multi-linear plots did not pass through the origin, suggesting that the adsorption rates of PFAS were not only limited by intra-particle diffusion, but also involved other steps, such as membrane diffusion and surface adsorption (Wang et al. 2016). The above findings revealed that PFAS adsorption may include chemical and physical processes. The adsorption rates of different PFAS varied depending on their molecular properties and followed the order of PFOA > 6:2 FTS > PFOS > PFHxA > GenX. PFAS with a carboxylate group, long chain or hydrocarbon bonds showed a faster adsorption process on MIL-101(Cr). The differential adsorption rates of PFAS may be attributed to the corresponding surface chemistry and molecular volume, and the PFAS diffusion in adsorption was likely to be negatively influenced by the binding with MIL-101(Cr) (Ateia et al. 2019).

225 **3.3 Adsorption isotherms of different PFAS**

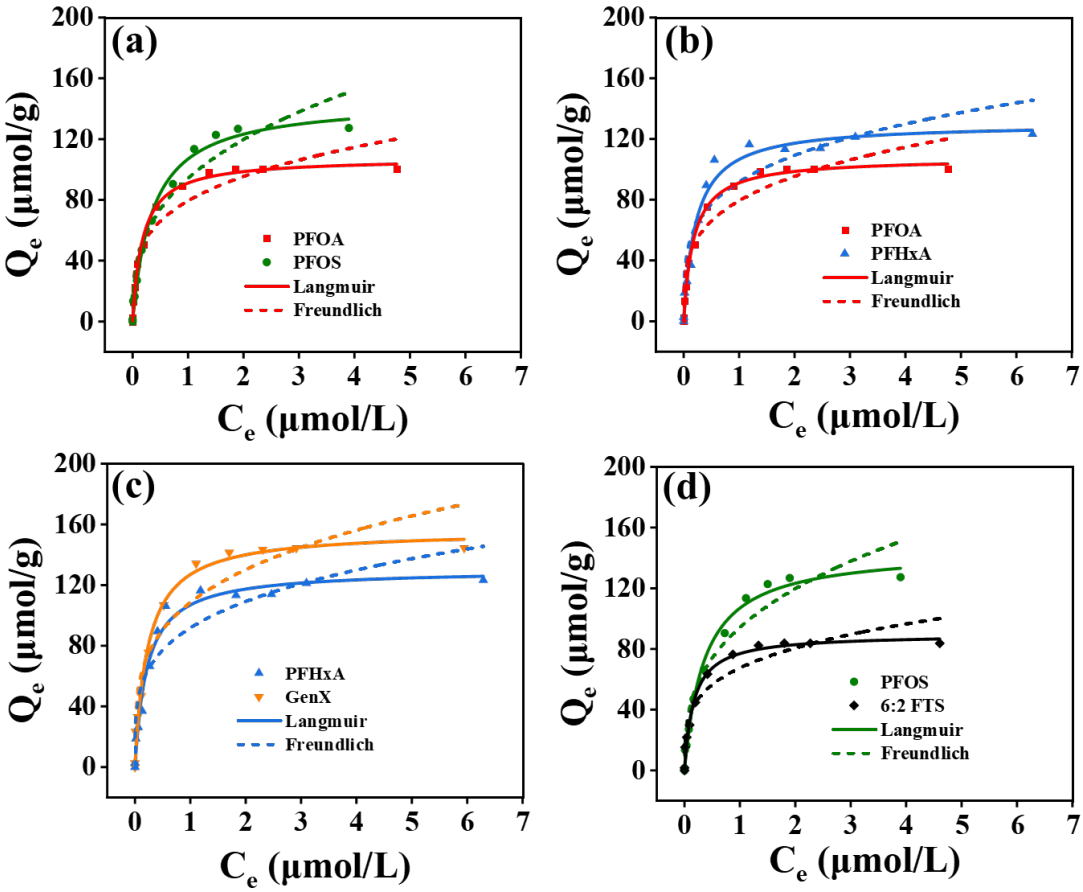

226

227 Fig. 2 Adsorption isotherms of PFOA, PFOS, PFHxA, GenX, and 6:2 FTS on MIL-101(Cr)

228 (solution pH: 5.0; adsorption duration: 24 h).

229 The maximum adsorption capacity (Q_m) fitted by the Langmuir isotherm

230 followed the order of GenX (156 μmol/g) > PFOS (145 μmol/g) > PFHxA (130 μmol/g) >

231 PFOA (107 μmol/g) > 6:2 FTS (89.7 μmol/g) (Table S6), and were associated with their

232 molecular characteristics. The PFAS with a sulfonate group, long chain, or ether bond

233 showed higher adsorption capacities on MIL-101(Cr), while replacing C-F units with

234 C-H units decreased the adsorption potential. The Q_m of PFOA was lower than that of

235 PFHxA, which could be due to the greater steric hindrance of micropores in MIL-

236 101(Cr) for longer-chain PFOA. For PFAS with the similar carbon chain lengths, the

much higher Q_m of GenX compared to PFHxA could likely be attributed to the decrease of steric effects by the branched carbon chain and the enhancement of hydrogen bonding by the introduced ether bond (Heidari et al. 2021), while replacing C-F units with less electronegative C-H units may diminish π-CF interaction of PFAS on MIL-101(Cr) leading to the lower adsorption capacity of 6:2 FTS than PFOS (Cheng et al. 2023). The sulfonate group in PFAS exhibited greater complexation with the Cr coordinatively unsaturated sites (CUS) of MOF compared with carboxylate group and thus resulted in the higher Q_m for PFOS compared to PFOA (Vecitis et al. 2009). In the Freundlich model fitting, all PFAS exhibited nonlinear adsorption isotherms (n<1) on MIL-101(Cr), indicating multiple mechanisms may exist during adsorption. The values of Gibbs free energy for the adsorption of various PFAS on MIL-101(Cr) were negative, indicating that these processes were spontaneous, and these Gibbs free energy values ranged in -20~0 kJ/mol (Fig. S4), suggesting that non-specific interactions played an important role during adsorption process (Yuan et al. 2023).

3.4 Effects of water matrix on the adsorption of different PFAS

3.4.1 Effects of pH

As solution pH increased from 4 to 10, the adsorption capacities of different PFAS on MIL-101(Cr) gradually declined (Fig. 3a). MIL-101(Cr) was found to be positively charged at low solution pH (less than the pH_{PZC} point of 6.85). An increase in solution pH can result in a decrease of zeta potentials and deprotonation for MIL-101(Cr), and thus lead to the weakening of electrostatic attraction and even increasing

258 electrostatic repulsion with anionic PFAS (Niece et al. 2003). It is noteworthy that the
259 magnitude of decline for PFAS adsorption also varied with their molecular
260 characteristics when solution pH increased. The F atoms on the fluorocarbon chain of
261 PFAS exhibited strong electronegativity and may contribute to the electrostatic
262 interaction with MIL-101(Cr) during adsorption. The adsorption process of PFAS with
263 longer fluorocarbon chains may depend more on electrostatic interactions, which thus
264 resulted in the PFOA adsorption being more affected by solution pH changes compared
265 with PFHxA. For the adsorption capacities of PFAS with similar fluorocarbon chain
266 lengths, as solution pH increased GenX showed a greater decline than PFHxA, which
267 was possibly due to the introduced ether bond of GenX increasing the hydrogen
268 bonding that was also affected by electrostatic interaction. Compared with PFOS,
269 replacing C-F units with C-H units diminishes the molecular electronegativity of 6:2
270 FTS, thus resulting in the lower sensitivity of 6:2 FTS adsorption to the varying solution
271 pH. The discrepancies in the adsorption capacities of PFOS and PFOA are mainly
272 related to the differential complexation potentials between sulfonate group or
273 carboxylate group of PFAS and Cr CUS of MIL-101(Cr), which may be less susceptible
274 to solution pH changes, therefore the magnitude of adsorption decline for PFOS and
275 PFOA were similar.

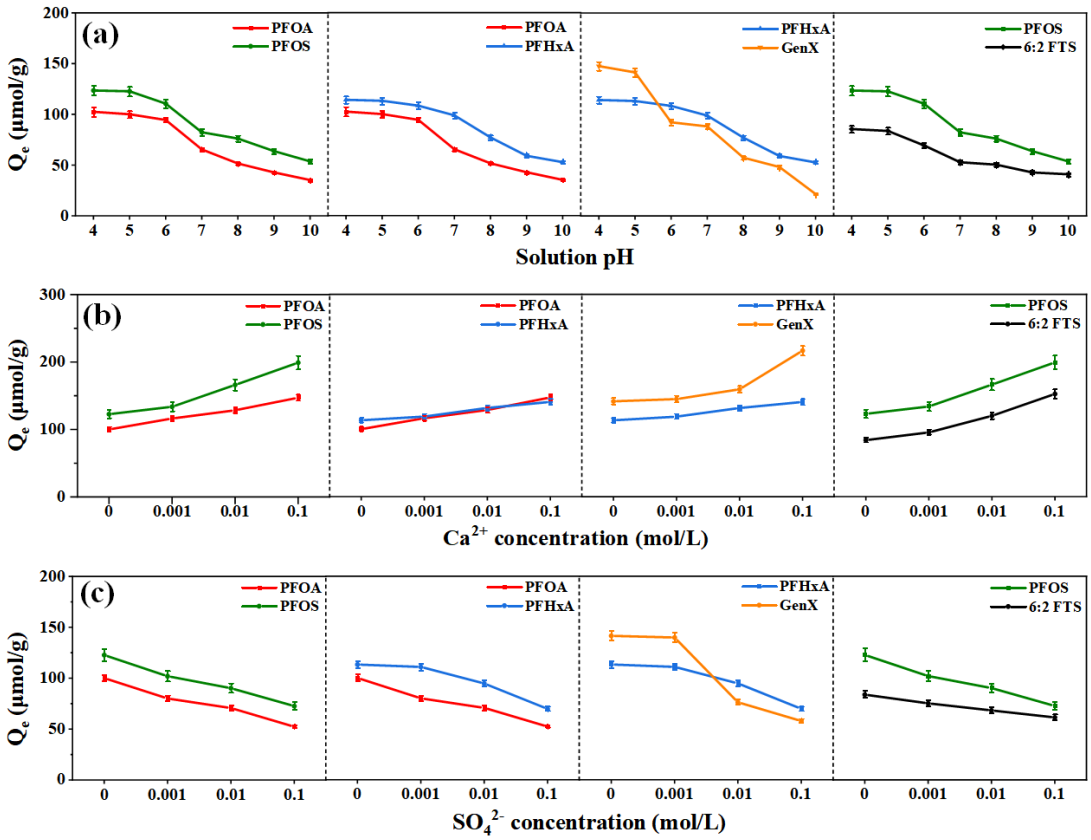

Fig. 3 Adsorption changes of different PFAS on MIL-101(Cr) under different solution pH (a) (solution pH: 4.0~10.0; adsorption duration: 24 h) and ionic strengths (solution pH: 5.0; adsorption duration: 24 h) of Ca^{2+} (b) and SO_4^{2-} (c).

3.4.2 Effects of ionic species and strength

The adsorption capacities of different PFAS on MIL-101(Cr) augmented with the increasing ionic strengths of Ca^{2+}, were mainly attributed to the promotion of cationic bridging (Fig. 3b) (Deng et al. 2010); while adsorption capacities declined as the ionic strengths of SO_4^{2-} increased, which could possibly have resulted from the competitive adsorption of SO_4^{2-} and anionic PFAS on MIL-101(Cr) (Fig. 3c) (Tan et al. 2023). The changes in ionic strength of Ca^{2+} and SO_4^{2-} exhibited a greater effect on the adsorption of PFAS with longer fluorocarbon chain or introduced ether bond, which

288 were likely associated with greater molecular electronegativities of these chemicals.
289 For PFAS with similar fluorocarbon chain lengths (e.g., PFOS and PFOA), the
290 sulfonate group showed greater electronegativity with a denser electron cloud and thus
291 higher bridging capacity with Ca^{2+} compared with the carboxylate group, which could
292 contribute to a greater increase in the adsorption of PFOS compared to PFOA as the
293 ionic strengths of Ca^{2+} increased (Liu et al. 2019); whereas with the increasing ionic
294 strength of SO_4^{2-}, the magnitude of adsorption decline for PFOS and PFOA were similar.
295 This could be due to the weak influence of SO_4^{2-} competitive adsorption on the
296 complexation between the sulfonate group or carboxylate group of PFAS and the Cr
297 CUS of MIL-101(Cr). In addition, the adsorption capacities of different PFAS on MIL-
298 101(Cr) exhibited a limited response to the changes of NaCl concentrations (Fig. S5).

3.5 Mechanism and prediction of PFAS adsorption

3.5.1 Adsorption mechanism of PFAS

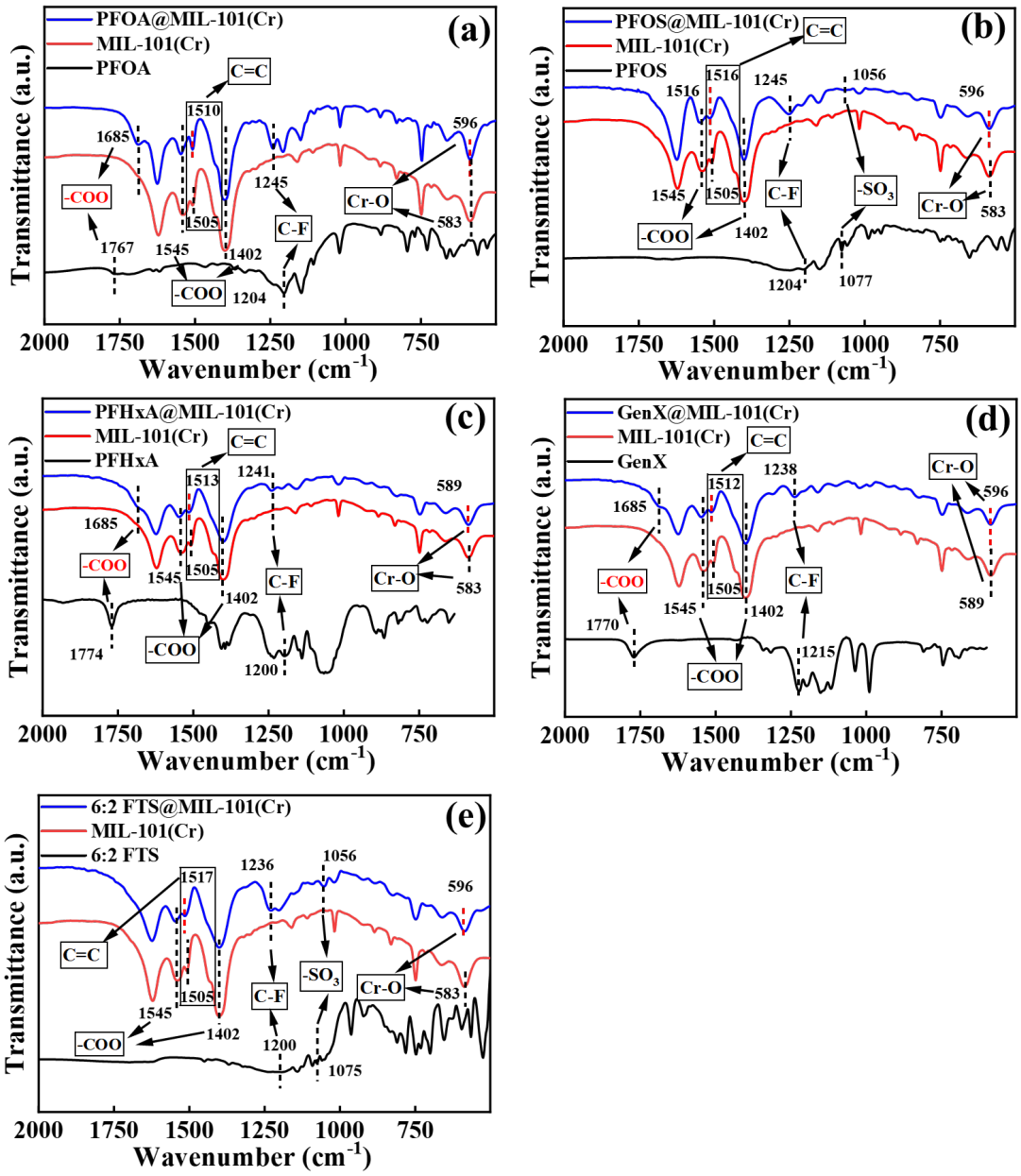

Fig. 4 FTIR spectra of MIL-101(Cr) before and after the adsorption of PFOA (a), PFOS (b), PFHxA (c), GenX (d), and 6:2 FTS (e), respectively.

The changes in functional groups of PFAS and MIL-101(Cr) during adsorption were analyzed via FTIR profiles to reveal the interaction mechanisms (Fig. 4). After

306 adsorption, the C-F peaks of PFOA (1204 cm^{-1}), PFOS (1204 cm^{-1}), PFHxA (1200 cm^{-1}), GenX (1215 cm^{-1}) and 6:2 FTS (1200 cm^{-1}) shifted to around 1245 cm^{-1}; the -COO peaks of PFOA (1767 cm^{-1}), PFHxA (1774 cm^{-1}), and GenX (1770 cm^{-1}) shifted to around 1685 cm^{-1}, and the $-SO_3$ of PFOS (1077 cm^{-1}) and 6:2 FTS (1075 cm^{-1}) shifted to around 1056 cm^{-1} (Gao and Chorover 2012). These observations indicated the interaction presence of the fluorocarbon chain and functional group of PFAS with the sorbent. Meanwhile, the aromatic carbon peak at 1505 cm^{-1} on the original MIL-101(Cr) varied after PFAS adsorption, which could be caused by the interactions of π-CF and π-anion (Liu et al. 2015, Mirsoleimani-azizi et al. 2018). Moreover, after absorbing PFOA, PFOS, PFHxA, GenX and 6:2 FTS, the peak of Cr-O on original MIL-101(Cr) (Bahadori et al. 2019) were shifted from 583 cm^{-1} to 596 cm^{-1}, 596 cm^{-1}, 589 cm^{-1}, 596 cm^{-1}, 596 cm^{-1}, respectively. This finding may be as a result of the complexation between the sulfonate or carboxylate group of PFAS and the Cr CUS of MIL-101(Cr). In addition, the peak intensity of -OH (3440 cm^{-1}) on MIL-101(Cr) were diminished after adsorbing PFAS, which could be related to hydrogen bonding between the sulfonate or carboxylate group of PFAS and the ligand water of Cr on MIL-101(Cr).

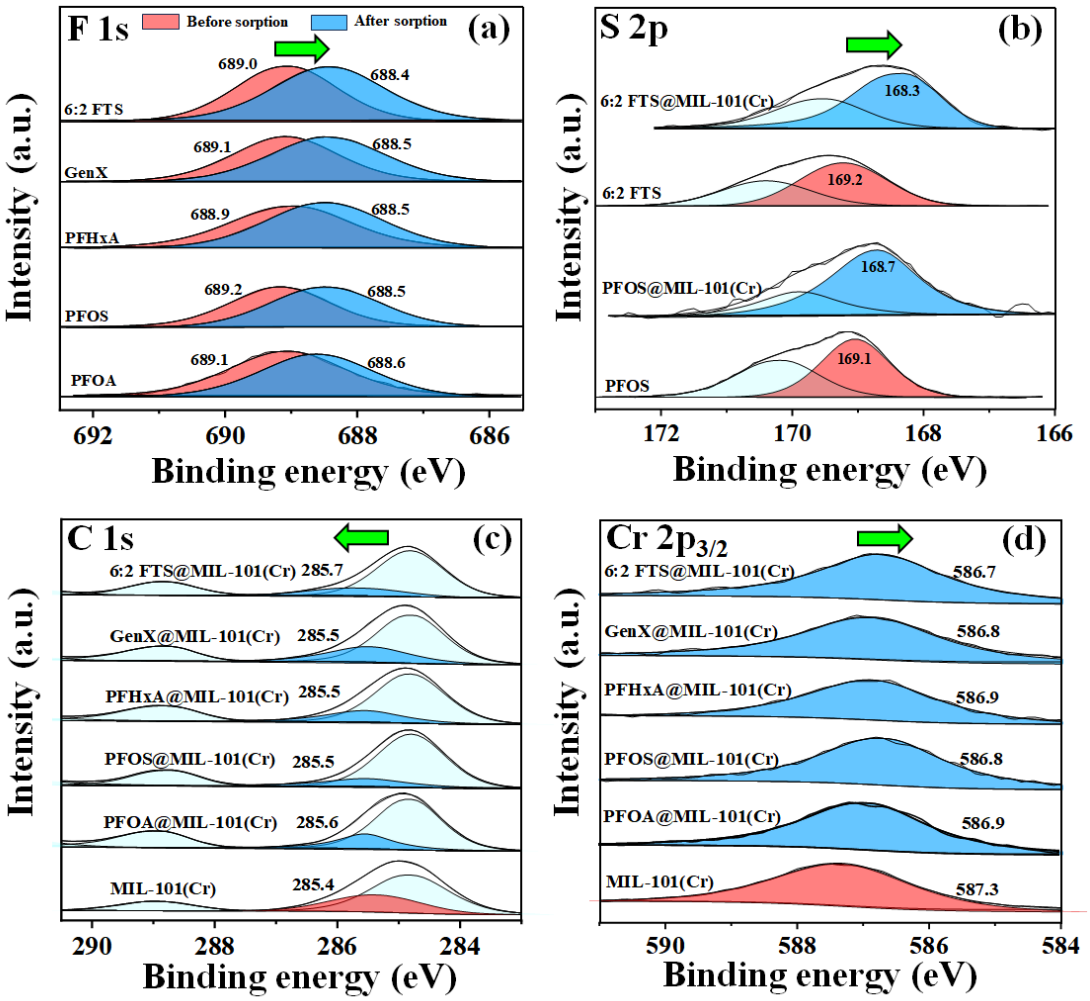

Fig. 5 XPS spectra of MIL-101(Cr) before and after the adsorption of PFOA (a), PFOS (b), PFHxA (c), GenX (d), and 6:2 FTS (e), respectively.

In order to further investigate the adsorption mechanism of different PFAS to MIL-101(Cr), XPS is used to observe the change of binding energy of PFAS and Fe-based MOFs before and after adsorption. According to the Fig. 5a, the appearance of high intensity peaks of F1 s means successful encapsulation of different PFAS to MIL-101(Cr). As shown in Fig. 5b, the binding energy for F of PFOA, PFOS, PFHxA, GenX and 6:2 FTS were 689.07 eV, 689.17 eV, 688.94 eV, 689.07 eV and 689.02 eV, respectively. After adsorption, the binding energies for F decrease, suggesting that the

C–F chain may have an interaction with the aromatic rings of MIL-101(Cr), which was supported by evidence of the shift of the C 1s aromatic ring at 285.4 eV for MIL-101(Cr). This finding indicated the F center gaining electron density in the adsorption of different PFAS on MIL-101(Cr), which demonstrated the interaction between C-F chain and MOF may be critical in the adsorption mechanism of PFAS (Barpaga et al. 2019). The S $2p_{3/2}$ peaks of original PFOS and 6:2 FTS shifted from 169.1 eV to 168.7 eV and from 169.2 eV to 168.3 eV respectively, when these chemicals were encapsulated onto MIL-101(Cr); while after the adsorption of PFOA, PFOS, PFHxA, GenX, and 6:2 FTS, the binding energies of Cr 2p3/2 on the original MIL-101(Cr) were shifted from 587.3 eV to 586.9, 586.8, 586.9, 586.8, and 586.7 eV, respectively. This observation may be further corroborated by the complexation between anion functional groups of PFAS and Cr CUS of MIL-101(Cr). Compared with coordinated H_2O, PFAS show a greater electronegativity, aiding the formation of coordinate bonds with Cr CUS of MIL-101(Cr) (Liu et al. 2015).

3.5.2 Adsorption prediction of PFAS

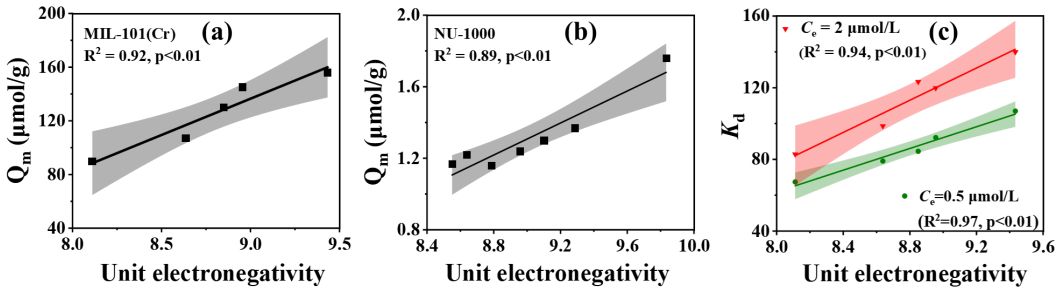

Fig. 6 Fitting between the unit electronegativity of individual PFAS and their Q_m values in MIL-101(Cr) of this study (a) and NU-1000 of a previous study (b), as well as fitting with the corresponding K_d values on MIL-101(Cr) (c).

351 Based on the results of the adsorption experiments and material characterization,
352 the adsorption mechanism of different PFAS on MIL-101(Cr) may involve electrostatic
353 interaction, complexation, hydrogen bonding, π-CF and π-anion, which are associated
354 with the binding energy influenced by the corresponding electron cloud density (Zhang
355 et al. 2021). The electron cloud density of different PFAS can be reflected by their
356 electronegativity that is mainly influenced by the peripheral atoms (e.g., F, O and H).
357 In addition, the kinetics reflected that PFAS adsorption was also influenced by the
358 diffusion and steric effects of these chemicals (Yang et al. 2020), which mainly
359 depended on their chain lengths. Considering the effects of PFAS molecular
360 electronegativity and chain lengths on adsorption, this study proposed a parameter of
361 average unit electronegativity (U_e), which was calculated by the electronegativity sum
362 of peripheral atoms (such as F, O and H) divided by the number of central atoms
363 (including C and S, and representing chain lengths) (Eq. 1), which aimed to provide an
364 adsorption capacity prediction of different PFAS on MOF.

365 $$U_e = \frac{F_n \times F_e + O_n \times O_e + H_n \times H_e}{C_n + S_n} \quad (1)$$

366 where U_e is the average unit electronegativity of PFAS, F_n, O_n, H_n, C_n and S_n
367 represent the atom electronegativity of F, O, H, C and S, respectively, and F_e, O_e, and
368 H_e represent the atom number of F, O and H, respectively.

369 The calculated U_e values of different PFAS followed the order of GenX (9.45) >
370 PFOS (8.98) > PFHxA (8.87) > PFOA (8.65) > 6:2 FTS (7.78), and were linearly and
371 positively correlated with their Q_m values (R^2>0.92, p<0.01) (Fig. 6a). Besides the

results of this study, a linear positive correlation between the U_e and Q_m values of various PFAS on NU-1000 has been reported in a previous study (Li et al. 2021) which was also found to support the feasibility of PFAS adsorption prediction on MOF by calculating U_e (Fig. 6b). Furthermore, the calculated U_e values of different PFAS also exhibited linear positive correlations with their adsorption coefficients (K_d) at different concentrations (C_e=0.5 and 2 μmol/L), which could be also used for removal rate predication of individual PFAS by MOF (Fig. 6a). Overall, this study attempted to develop a novel strategy for PFAS adsorption prediction on MOF based on their molecular properties.

4. Practical applications and recycling of MIL-101(Cr) in natural water

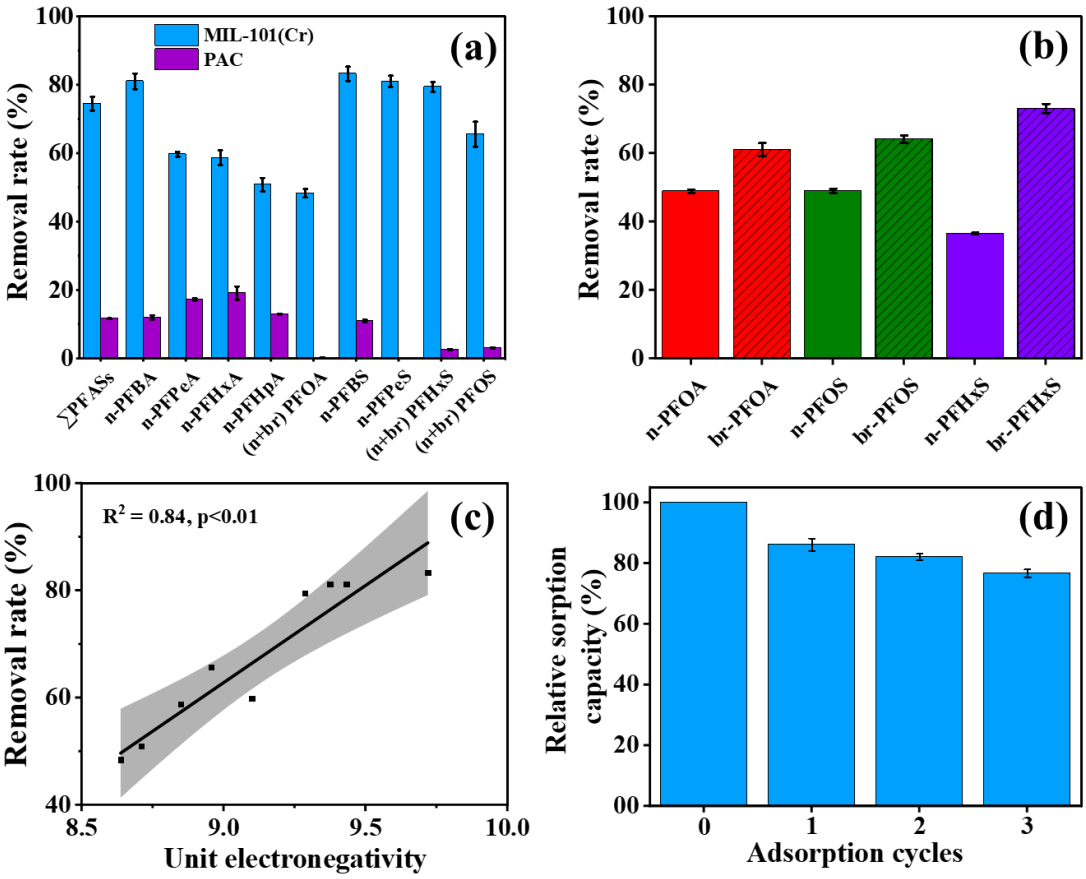

Fig. 7 Removal rates (a, b) and unit electronegativity-based fitting (c) of major PFAS by MIL-

384 101(Cr) in natural water, as well as their relative adsorption capacities in three cycling experiments
385 (d). (solution pH: 8.0; adsorption duration: 24 h; n represent linear isomer, br represent branched
386 isomer).

387 A heavily-polluted groundwater sample containing nine major PFAS (∑PFAS:
388 114 μg/L) collected from a nearby a fluorochemical facility was used to examine the
389 practical application of MIL-101(Cr) (Fig. 7a). The total removal rate of PFAS by 0.8
390 mg/L of MIL-101(Cr) reached up to approximately 75%, and much higher than that
391 (about 10%) by the same sorbent concentration of commercial powdered activated
392 carbon (PAC). Consistent with the results of adsorption experiments, MIL-101(Cr)
393 generally showed higher removal rates for PFAS with a sulfonate group, long chain, or
394 ether bond, and the removal rate of major PFAS also demonstrated a significantly
395 positive correlation with their U_e values (R^2>0.84, p<0.01) (Fig. 7c). It is worth
396 mentioning that the removal rates of branched-chain PFAS by MIL-101(Cr) were
397 higher than those of corresponding linear isomers, which were supported by evidence
398 from the isomer removal rates of PFOA (br-PFOA: 61%; n-PFOA: 49%), PFOS (br-
399 PFOS: 64%; n-PFOS: 49%) and perfluorohexane sulfonate (PFHxS) (br-PFHxS: 73%;
400 n-PFHxS: 37%) (Fig. 7b). This finding may be due to lower steric effects and higher
401 number of interaction sites during the adsorption of branched PFAS compared to their
402 linear isomers (Kim et al. 2023). Based on the physicochemical properties of PFAS and
403 the ionic effects on their adsorption, a methanol solution containing 1.25% $NaNO_3$,
404 1.25% NaCl, 1.25% Na_2SO_4 and 1.25% Na_2CO_3 was developed to efficiently elute the

405 sorbed PFAS from MIL-101(Cr) to achieve the material regeneration. The superior
406 regeneration of MIL-101(Cr) was verified by performing three consecutive recycling
407 experiments in the natural water sample, with the relative adsorption capacities of Σ
408 PFAS still remaining over 80% (Fig. 7d). The notable adsorption efficiencies of MIL-
409 101(Cr) for multiple PFAS in natural waters and its recycling performance suggest it,
410 and MOF counterparts, may be te promising sorbents for the treatment of PFAS-
411 contaminated water.

412 **5. Conclusions and perspectives**

413 Legacy PFOS and PFOA are being replaced by short-chain homologs and novel
414 alternatives. However, there has been limited research on the effects of varying carbon
415 chains and functional groups of PFAS on their adsorption by sorbents such as MOF.
416 This study has systematically assessed the structure-adsorption relationships and
417 interaction mechanisms of legacy and emerging PFAS on MIL-101(Cr), and as a result
418 proposed a parameter reflecting average unit electronegativity for PFAS adsorption
419 prediction. Our findings demonstrate that PFAS with a sulfonate group, long chain, or
420 ether bond (e.g., GenX) show higher adsorption capacities on MIL-101(Cr), while
421 replacing C-F units with C-H units can decrease the adsorption potential of PFAS (e.g.,
422 6:2 FTS). Divalent cation (such as Ca^{2+}) may promote PFAS adsorption on MIL-101(Cr)
423 via cationic bridging with negatively charged PFAS, while the increase of pH and
424 divalent anion (such as SO_4^{2-}) could inhibit adsorption by weakening electrostatic
425 attraction and enhancing competitive adsorption, respectively. The adsorption

426 processes of structurally different PFAS are mainly governed by electrostatic
427 interaction, complexation, hydrogen bonding, π-CF and π-anion (which are associated
428 with PFAS molecular electronegativities). They are also influenced by diffusion and
429 steric effects which are mainly dependent on PFAS chain lengths. Considering the
430 effects of PFAS molecular electronegativity and chain length on adsorption, a parameter
431 of average unit electronegativity of PFAS (named as U_e) was found to show
432 significantly positive correlations with adsorption capacities and removal rates of
433 individual PFAS on MIL-101(Cr). The adsorption efficiencies of branched PFAS by
434 MIL-101(Cr) were found to be higher compared to corresponding linear isomers,
435 possibly due to the lower steric effects and more interaction sites during adsorption of
436 branched PFAS.

437 The notable adsorption efficiencies and recycling performance of MIL-101(Cr)
438 for the removal of multiple PFAS in natural waters was verified, making it and MOF
439 counterparts, potentially promising sorbents for the treatment of PFAS-contaminated
440 waters. The adsorption mechanisms of different structural PFAS and thus proposed U_e
441 values can provide critical information for the adsorption prediction of PFAS on MOFs,
442 which would aid tailoring the development and modification of efficient MOFs
443 according to the specific contamination characters of environmental PFAS. As the range
444 and type of PFAS have increased in recent years, this study should provide a helpful
445 approach to facilitate the adsorption prediction of individual PFAS on MOF based on
446 their molecular structures and interaction mechanisms. This will enable future studies

to focus on more detailed interaction mechanisms and integrating more molecular properties of PFAS to achieve a more precise prediction of adsorption.

References

Ateia, M., Alsbaiee, A., Karanfil, T. and Dichtel, W. (2019) Efficient PFAS Removal by Amine-Functionalized Sorbents: Critical Review of the Current Literature. Environmental Science & Technology Letters 6(12), 688-695.

Bahadori, M., Tangestaninejad, S., Bertmer, M., Moghadam, M., Mirkhani, V., Mohammadpoor−Baltork, I., Kardanpour, R. and Zadehahmadi, F. (2019) Task-Specific Ionic Liquid Functionalized–MIL–101(Cr) as a Heterogeneous and Efficient Catalyst for the Cycloaddition of CO2 with Epoxides Under Solvent Free Conditions. ACS Sustainable Chemistry & Engineering 7(4), 3962-3973.

Barpaga, D., Zheng, J., Han, K.S., Soltis, J.A., Shutthanandan, V., Basuray, S., McGrail, B.P., Chatterjee, S. and Motkuri, R.K. (2019) Probing the Sorption of Perfluorooctanesulfonate Using Mesoporous Metal–Organic Frameworks from Aqueous Solutions. Inorganic Chemistry 58(13), 8339-8346.

Cheng, J.H., Liang, X.Y., Yang, S.W. and Hu, Y.Y. (2014) Photochemical defluorination of aqueous perfluorooctanoic acid (PFOA) by VUV/Fe^{3+} system. Chemical Engineering Journal 239, 242-249.

Cheng, X., Liu, L., Ge, Y., Weber, R. and Huang, J. (2023) Target and non-target analysis of per- and polyfluoroalkyl substances in representative chrome mist suppressants on the Chinese market. Chemosphere 337.

Deng, S., Nie, Y., Du, Z., Huang, Q., Meng, P., Wang, B., Huang, J. and Yu, G. (2015) Enhanced adsorption of perfluorooctane sulfonate and perfluorooctanoate by bamboo-derived granular activated carbon. J Hazard Mater 282, 150-157.

Deng, S., Yu, Q., Huang, J. and Yu, G. (2010) Removal of perfluorooctane sulfonate from wastewater by anion exchange resins: effects of resin properties and solution chemistry. Water Res 44(18), 5188-5195.

Du, Z., Deng, S., Bei, Y., Huang, Q., Wang, B., Huang, J. and Yu, G. (2014) Adsorption behavior and mechanism of perfluorinated compounds on various adsorbents--a review. J Hazard Mater 274, 443-454.

Fakhraie, S., Rajabi, H.R. and Rashidi, A. (2023) Fabrication and application of novel core–shell MIL-101(Cr)@UiO-66(Zr) nanocrystals for highly selective separation of H2S and CO2. Chemical Engineering Journal 452.

Fang, Y., Meng, P., Schaefer, C. and Knappe, D.R.U. (2023) Removal and destruction of perfluoroalkyl ether carboxylic acids (PFECAs) in an anion exchange resin and electrochemical oxidation

treatment train. Water Res 230, 119522.

FitzGerald, L.I., Olorunyomi, J.F., Singh, R. and Doherty, C.M. (2022) Towards Solving the PFAS Problem: The Potential Role of Metal‐Organic Frameworks. ChemSusChem 15(19).

Gao, X. and Chorover, J. (2012) Adsorption of perfluorooctanoic acid and perfluorooctanesulfonic acid to iron oxide surfaces as studied by flow-through ATR-FTIR spectroscopy. Environmental Chemistry 9(2).

Gomis, M.I., Vestergren, R., Borg, D. and Cousins, I.T. (2018) Comparing the toxic potency in vivo of long-chain perfluoroalkyl acids and fluorinated alternatives. Environ Int 113, 1-9.

Heidari, H., Abbas, T., Ok, Y.S., Tsang, D.C.W., Bhatnagar, A. and Khan, E. (2021) GenX is not always a better fluorinated organic compound than PFOA: A critical review on aqueous phase treatability by adsorption and its associated cost. Water Research 205.

Joerss, H., Xie, Z., Wagner, C.C., von Appen, W.J., Sunderland, E.M. and Ebinghaus, R. (2020) Transport of Legacy Perfluoroalkyl Substances and the Replacement Compound HFPO-DA through the Atlantic Gateway to the Arctic Ocean-Is the Arctic a Sink or a Source? Environ Sci Technol 54(16), 9958-9967.

Kim, Y., Pike, K.A., Gray, R., Sprankle, J.W., Faust, J.A. and Edmiston, P.L. (2023) Non-targeted identification and semi-quantitation of emerging per- and polyfluoroalkyl substances (PFAS) in US rainwater. Environmental Science: Processes & Impacts.

Li, H., Junker, A.L., Wen, J., Ahrens, L., Sillanpää, M., Tian, J., Cui, F., Vergeynst, L. and Wei, Z. (2023) A recent overview of per- and polyfluoroalkyl substances (PFAS) removal by functional framework materials. Chemical Engineering Journal 452.

Li, R., Alomari, S., Stanton, R., Wasson, M.C., Islamoglu, T., Farha, O.K., Holsen, T.M., Thagard, S.M., Trivedi, D.J. and Wriedt, M. (2021) Efficient Removal of Per- and Polyfluoroalkyl Substances from Water with Zirconium-Based Metal–Organic Frameworks. Chemistry of Materials 33(9), 3276-3285.

Li, Y., Braunig, J., Thai, P.K., Rebosura, M., Mueller, J.F. and Yuan, Z. (2022) Formation and fate of perfluoroalkyl acids (PFAAs) in a laboratory-scale urban wastewater system. Water Res 216, 118295.

Li, Y., Yang, Z., Wang, Y., Bai, Z., Zheng, T., Dai, X., Liu, S., Gui, D., Liu, W., Chen, M., Chen, L., Diwu, J., Zhu, L., Zhou, R., Chai, Z., Albrecht-Schmitt, T.E. and Wang, S. (2017) A mesoporous cationic thorium-organic framework that rapidly traps anionic persistent organic pollutants. Nat Commun 8(1), 1354.

Liu, K., Zhang, S., Hu, X., Zhang, K., Roy, A. and Yu, G. (2015) Understanding the Adsorption of PFOA

515 on MIL-101(Cr)-Based Anionic-Exchange Metal-Organic Frameworks: Comparing DFT
516 Calculations with Aqueous Sorption Experiments. Environ Sci Technol 49(14), 8657-8665.
517 Liu, L., Liu, Y., Gao, B., Ji, R., Li, C. and Wang, S. (2019) Removal of perfluorooctanoic acid (PFOA)
518 and perfluorooctane sulfonate (PFOS) from water by carbonaceous nanomaterials: A review.
519 Critical Reviews in Environmental Science and Technology 50(22), 2379-2414.
520 Liu, Q., Ning, L., Zheng, S., Tao, M., Shi, Y. and He, Y. (2013) Adsorption of Carbon Dioxide by MIL-
521 101(Cr): Regeneration Conditions and Influence of Flue Gas Contaminants. Scientific Reports
522 3(1).
523 Liu, X., Zhu, C., Yin, J., Li, J., Zhang, Z., Li, J., Shui, F., You, Z., Shi, Z., Li, B., Bu, X.H., Nafady, A.
524 and Ma, S. (2022) Installation of synergistic binding sites onto porous organic polymers for
525 efficient removal of perfluorooctanoic acid. Nat Commun 13(1), 2132.
526 Lu, N., Wang, T., Zhao, P., Zhang, L., Lun, X., Zhang, X. and Hou, X. (2016) Experimental and molecular
527 docking investigation on metal-organic framework MIL-101(Cr) as a sorbent for vortex assisted
528 dispersive micro-solid-phase extraction of trace 5-nitroimidazole residues in environmental
529 water samples prior to UPLC-MS/MS analysis. Analytical and Bioanalytical Chemistry 408(29),
530 8515-8528.
531 Ma, D., Lu, Y., Liang, Y., Ruan, T., Li, J., Zhao, C., Wang, Y. and Jiang, G. (2022) A Critical Review on
532 Transplacental Transfer of Per- and Polyfluoroalkyl Substances: Prenatal Exposure Levels,
533 Characteristics, and Mechanisms. Environ Sci Technol 56(10), 6014-6026.
534 Maksimchuk, N., Timofeeva, M., Melgunov, M., Shmakov, A., Chesalov, Y., Dybtsev, D., Fedin, V. and
535 Kholdeeva, O. (2008) Heterogeneous selective oxidation catalysts based on coordination
536 polymer MIL-101 and transition metal-substituted polyoxometalates. Journal of Catalysis
537 257(2), 315-323.
538 Mirsoleimani-azizi, S.M., Setoodeh, P., Samimi, F., Shadmehr, J., Hamedi, N. and Rahimpour, M.R.
539 (2018) Diazinon removal from aqueous media by mesoporous MIL-101(Cr) in a continuous
540 fixed-bed system. Journal of Environmental Chemical Engineering 6(4), 4653-4664.
541 Nickerson, A., Rodowa, A.E., Adamson, D.T., Field, J.A., Kulkarni, P.R., Kornuc, J.J. and Higgins, C.P.
542 (2021) Spatial Trends of Anionic, Zwitterionic, and Cationic PFASs at an AFFF-Impacted Site.
543 Environ Sci Technol 55(1), 313-323.
544 Peng, Y.-P., Chen, H. and Huang, C.P. (2017) The Synergistic Effect of Photoelectrochemical (PEC)
545 Reactions Exemplified by Concurrent Perfluorooctanoic acid (PFOA) Degradation and
546 Hydrogen Generation over Carbon and Nitrogen codoped TiO 2 Nanotube Arrays (C-N-TNTAs)
547 photoelectrode. Applied Catalysis B: Environmental 209, 437-446.

Piai, L., Dykstra, J.E., Adishakti, M.G., Blokland, M., Langenhoff, A.A.M. and van der Wal, A. (2019) Diffusion of hydrophilic organic micropollutants in granular activated carbon with different pore sizes. Water Res 162, 518-527.

Rosler, C., Aijaz, A., Turner, S., Filippousi, M., Shahabi, A., Xia, W., Van Tendeloo, G., Muhler, M. and Fischer, R.A. (2016) Hollow Zn/Co Zeolitic Imidazolate Framework (ZIF) and Yolk-Shell Metal@Zn/Co ZIF Nanostructures. Chemistry 22(10), 3304-3311.

Schulz, K., Silva, M.R. and Klaper, R. (2020) Distribution and effects of branched versus linear isomers of PFOA, PFOS, and PFHxS: A review of recent literature. Sci Total Environ 733, 139186.

Sun, X., Xia, Q., Zhao, Z., Li, Y. and Li, Z. (2014) Synthesis and adsorption performance of MIL-101(Cr)/graphite oxide composites with high capacities of n-hexane. Chemical Engineering Journal 239, 226-232.

Tan, X., Jiang, Z., Ding, W., Zhang, M. and Huang, Y. (2023) Multiple interactions steered high affinity toward PFAS on ultrathin layered rare-earth hydroxide nanosheets: Remediation performance and molecular-level insights. Water Research 230.

Vecitis, C.D., Park, H., Cheng, J., Mader, B.T. and Hoffmann, M.R. (2009) Treatment technologies for aqueous perfluorooctanesulfonate (PFOS) and perfluorooctanoate (PFOA). Frontiers of Environmental Science & Engineering in China 3(2), 129-151.

Wang, H., Hu, D., Wen, W., Lin, X. and Xia, X. (2023) Warming Affects Bioconcentration and Bioaccumulation of Per- and Polyfluoroalkyl Substances by Pelagic and Benthic Organisms in a Water-Sediment System. Environ Sci Technol 57(9), 3612-3622.

Wang, T., Zhao, P., Lu, N., Chen, H., Zhang, C. and Hou, X. (2016) Facile fabrication of Fe 3 O 4 /MIL-101(Cr) for effective removal of acid red 1 and orange G from aqueous solution. Chemical Engineering Journal 295, 403-413.

Wang, W., Maimaiti, A., Shi, H., Wu, R., Wang, R., Li, Z., Qi, D., Yu, G. and Deng, S. (2019) Adsorption behavior and mechanism of emerging perfluoro-2-propoxypropanoic acid (GenX) on activated carbons and resins. Chemical Engineering Journal 364, 132-138.

Yang, Y., Zheng, Z., Ji, W., Xu, J. and Zhang, X. (2020) Insights to perfluorooctanoic acid adsorption micro-mechanism over Fe-based metal organic frameworks: Combining computational calculation with response surface methodology. Journal of Hazardous Materials 395.

Yu, B., Liu, Y., Li, Z., Liu, Y., Rao, P. and Li, G. (2023) Durable substrates incorporated with MOFs: Recent advances in engineering strategies and water treatment applications. Chemical Engineering Journal 455.

Yuan, S., Wang, X., Jiang, Z., Zhang, H. and Yuan, S. (2023) Contribution of air-water interface in

removing PFAS from drinking water: Adsorption, stability, interaction and machine learning studies. Water Research 236.

Zhang, T., Zheng, L., Yu, H., Ren, J., Peng, D., Zhang, L. and Meng, P. (2021) Multiple adsorption systems and electron-scale insights into the high efficiency coadsorption of a novel assembled cellulose via experiments and DFT calculations. Journal of Hazardous Materials 416.

Zhao, C., Xu, Y., Xiao, F., Ma, J., Zou, Y. and Tang, W. (2021) Perfluorooctane sulfonate removal by metal-organic frameworks (MOFs): Insights into the effect and mechanism of metal nodes and organic ligands. Chemical Engineering Journal 406.

Zhao, H., Li, Q., Wang, Z., Wu, T. and Zhang, M. (2020) Synthesis of MIL-101(Cr) and its water adsorption performance. Microporous and Mesoporous Materials 297.